HHS Public Access

Author manuscript

ACS Chem Biol. Author manuscript; available in PMC 2018 April 21.

Published in final edited form as:

ACS Chem Biol. 2017 April 21; 12(4): 1066–1074. doi:10.1021/acschembio.6b00883.

The GCaMP-R Family of Genetically Encoded Ratiometric Calcium Indicators

Jung-Hwa Cho[†,iD], **Carter J. Swanson**[‖,iD], **Jeannie Chen**[‡], **Ang Li**[§], **Lisa G. Lippert**[⊥], **Shannon E. Boye**[#], **Kasey Rose**[‡], **Sivaraj Sivaramakrishnan**[⊥], **Cheng-Ming Chuong**[§], and **Robert H. Chow**[*,†,∇]

[†]Department of Physiology and Biophysics, Keck School of Medicine, University of Southern California, Los Angeles, California 90033, United States

[‡]Department of Cell & Neurobiology, Keck School of Medicine, University of Southern California, Los Angeles, California 90033, United States

[§]Department of Pathology, Keck School of Medicine, University of Southern California, Los Angeles, California 90033, United States

[‖]Biophysics Program, University of Michigan, 930 N. University, Room 4028, Ann Arbor, Michigan 48109, United States

[⊥]Department of Genetics, Cell Biology & Development, University of Minnesota Twin Cities, 4-130 MCB, 420 Washington Avenue SE, Minneapolis, Minnesota 55455, United States

[#]Department of Ophthalmology, University of Florida, 2000 SW Archer Rd, Rm R3-128, Gainesville, Florida 32611, United States

[∇]Department of Biomedical Engineering, Zilkha Neurogenetic Institute, University of Southern California, Room 323, Keck School of Medicine, Los Angeles, California 90089, United States

Abstract

We report on GCaMP-Rs, a new family of genetically encoded ratiometric calcium indicators that extend the virtues of the GCaMP proteins to ratiometric measurements. We have engineered a tandem construct of calcium-dependent GCaMP and calcium-independent mCherry fluorescent

[*]**Corresponding Author**: Tel.: 323-442-2901. Fax: 323-442-4466. rchow@med.usc.edu.

ORCID

Jung-Hwa Cho: 0000-0002-9041-3081

Carter J. Swanson: 0000-0001-6697-9475

ASSOCIATED CONTENT

Supporting Information

The Supporting Information is available free of charge on the ACS Publications website at DOI: 10.1021/acschem-bio.6b00883.

Movie S1 (AVI)

Movie S2 (AVI)

Movie S3 (AVI)

Movie S4 (AVI)

Detailed experimental procedures and five supplementary figures (PDF)

The authors declare no competing financial interest.

proteins. The tandem design assures that the two proteins localize in the same cellular compartment(s) and facilitates pixelwise ratiometric measurements; however, Förster resonance energy transfer (FRET) between the fluorophores reduces brightness of the sensor by up to half (depending on the GCaMP variant). To eliminate FRET, we introduced a rigid α-helix, the ER/K helix, between GCaMP and mCherry. Avoiding FRET significantly increases the brightness (notably, even at low calcium concentrations), the signal-to-noise ratio, and the dynamic range.

Graphical abstract

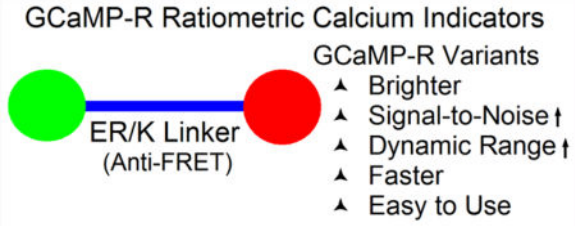

The synthetic calcium dyes Fura-2 and Indo-1 have long been available for quantitative monitoring of intracellular calcium dynamics in living cells.[1] Binding of calcium ions causes a shift in the peak of the excitation spectrum for Fura-2 and of the emission spectrum for Indo-1.[2] The ratio of fluorescence emission intensities for one (Indo-1) or two excitation wavelengths (Fura-2) is a highly reproducible function of the free calcium concentration; thus, these “ratiometric” dyes can be used to quantify free calcium concentration. Their use is, however, limited to short-duration experiments, as the dyes are eliminated from the cytoplasm.[3,4] Moreover, they are not ideal for deep tissue calcium imaging, because both dyes require ultraviolet (UV) excitation light, which has less penetration depth than visible wavelengths and, in addition, is phototoxic. Furthermore, targeting specific cells or subcellular locations for measurements is not so readily achieved with synthetic dyes as with genetically encoded calcium indicators (GECIs), whose expression can be targeted to specific cells and even specific subcellular regions.[5–7]

Among GECIs, GCaMP variants are widely used for live cell and in vivo calcium imaging.[8,9] GCaMP3[10] is composed of a calcium binding protein calmodulin (CaM), a CaM-binding domain RS20 derived from smooth muscle myosin light chain kinase, and a circularly permuted (cp) green fluorescent protein (cpGFP). Upon calcium elevation and binding to CaM, an intramolecular interaction between calcium-bound CaM and RS20 at C-terminal and N-terminal ends of cpGFP leads to protection of the cpGFP chromophore from aqueous solutions, thereby increasing emission fluorescence intensity. Subsequent improvement of GCaMPs eventually led to GCaMP6 variants that are sufficiently bright and fast enough to report cytoplasmic calcium changes due to single action potentials.[11] However, their fluorescence is nearly absent at basal calcium levels, making it difficult to determine whether expression has been successful. Furthermore, the intensity changes without a spectral shift when calcium concentration changes, and the peak fluorescence intensity also varies with expression levels, making them unsuitable for quantitative ratiometric measurements. Random mutagenesis of GCaMP3 led to the development of Fura-2-like (GEX-GECO1) and Indo-1-like (GEM-GECO1)—two early genetically encoded

ratiometric calcium indicators (GE"**R**"CIs), which, however, require near-UV excitation wavelengths,[12] limiting imaging to shallow tissue depths. REX-GECO variants are excited at visible wavelengths and exhibit a shift in excitation wavelength between the calcium-free to calcium-bound states.[13] However, the peak of the excitation spectra in the absence of calcium is similar to the peak of the emission spectra in $CaCl_2$ solution, making ratiometric calcium imaging difficult.

Another class of GERCIs exploits changes in the efficiency of Förster resonance energy transfer (FRET) between donor and acceptor fluorescent proteins separated by protein domains that change conformation upon binding to calcium—*e.g.*, calmodulin or troponin C (TnC). Early FRET indicators (*e.g.*, D4cpv[14] and TN-XXL[15]) provided quantitative estimates of calcium concentration, however, were limited by slow response kinetics. More recently, TnC-based FRET sensor variants (Twitch[16]) have been developed that offer linear response, smaller size, a wider range of calcium affinity, better photostability, larger dynamic range, and faster kinetics compared to their predecessor TN-XXL. Even after these improvements, however, the FRET sensors still suffer from low signal-to-noise ratios (SNR), due to the stringent demands of efficient FRET. Compared with the on- and off-response kinetics of GCaMP variants, the off-rate of Twitch is still significantly slower.[17,18] Moreover, FRET calcium sensors require extensive post data processing to extract the spectral contributions of donor and acceptor proteins, in order to obtain accurate FRET ratios.

RESULTS AND DISCUSSION

ER/K α-Helix Linker Prevents FRET

For a tandem construct consisting of GCaMP attached to mCherry, the ratio of GCaMP to mCherry fluorescence should be a highly reproducible function of free calcium concentration. The tandem design, however, raises the possibility that GCaMP and mCherry may undergo FRET, as mCherry's excitation and GCaMP's emission spectra overlap (Figure 1A), and FRET would reduce the donor/acceptor fluorescence ratio. Separating the fluorophores by a rigid α-helix should prevent FRET.[19] The ER/K α-helix is a rigid helix composed of tandem repeats of four glutamic acids (E) followed by four arginine (R) or lysine (K) residues. It maintains α-helical structure in solution due to strategic side-chain charge—charge interactions.[20] As we show below, incorporating an ER/K spacer/linker of 30 nm length—much longer than the 5.4 nm Förster radius for EGFP-mCherry[21]—prevents FRET and significantly increases the GCaMP/mCherry ratio. We have named the family of new genetically encoded ratiometric calcium sensors the "GCaMP-R" family—as in, GCaMP-R-3, GCaMP-R-6s, and GCaMP-R-6f, where the suffix indicates the GCaMP variant.

The advantage of using the ER/K linker was tested by generating a range of constructs with GCaMP connected to mCherry by different linkers. The different tandem constructs are here designated "#-linker," in which # refers to the GCaMP variant (we used GCaMP3, GCaMP6s, and GCaMP6f, so # would be 3, 6s, or 6f), and the linker is denoted by one of the following: ER/K refers to the ER/K helix, DELTA to a linker composed of 18 amino acids (EFGSGENLYFQGGSGGAP), and GS to a linker consisting of the peptide GSGSGS.

Thus, for example, “3-ER/K” denotes GCaMP3 linked *via* an ER/K α-helix to mCherry; “3-DELTA” denotes GCaMP3 linked to mCherry by the DELTA peptide; “3-GS” denotes GCaMP3 linked to mCherry by the GS peptide. All the #-ER/K and #-DELTA linkers contain a Tobacco Etch Virus (TEV) protease cleavage site (Figures 1B and 2A).

Figure 1C—H show *in vitro* spectra of purified GERCIs. Emission spectra of the purified tandem GCaMP3 and mCherry proteins were measured using a spectrofluorometer. GCaMP3 was excited directly at the 485 nm wavelength, and mCherry at 587 nm. The emission spectra of GCaMP3 and mCherry of the 3-ER/K, 3-DELTA, and 3-GS sensor were measured in 1 mM $CaCl_2$, with and without 0.5 μM TEV protease. mCherry fluorescence excited at 587 nm and measured at 608 nm was used to normalize the emission spectra of GCaMP3, allowing quantitative comparison of the tandem sensors (Figure 1E,H). The peak ratio of GCaMP3 fluorescence divided by mCherry fluorescence for 3-ER/K in 1 mM $CaCl_2$ was greater than that of 3-DELTA by 40% and greater than that of 3-GS by 37% (Figure 1K). After the treatment with TEV protease, the peak values of 3-ER/K and 3-DELTA became equal, as expected if FRET had been eliminated—the peak value of 3-ER/K was reduced by 13%, due to partial quenching of fluorescence by TEV protease,[19] while for 3-DELTA, the peak was increased by 19%. The treatment with TEV protease had no effect on the ratio for 3-GS, as expected, since 3-GS does not have a TEV cleavage site.

Insets in Figure 1E and H show magnified spectra centered around 610 nm and illustrate that the bump in mCherry emission around 600 nm is due to FRET between GCaMP3 and mCherry in the FRET-permissive constructs. After the treatment with TEV protease, the bump in the 3-DELTA spectrum disappeared so that the 3-DELTA and the 3-ER/K spectra at 600 nm became superimposed, and the fluorescence of 3-DELTA at 511 nm increased. However, the 3-GS spectrum remained the same. Taken together, these data show that separating GCaMP3 and mCherry in 3-DELTA eliminated FRET. Following the spectral measurements, the protein samples were run on a gel, verifying cleavage by TEV protease (Figure 1I,J). Note that after the ER/K and DELTA sensors were treated with TEV protease, the protein bands for GCaMP3 were located near that of GCaMP3 alone, while the position of GCaMP3 bands in GS sensors remained unchanged.

ER/K α-Helix Linker Increases GCaMP Signals *in Vitro*

Next, we tested out not only GCaMP3 tandem sensors but also GCaMP6s and GCaMP6f tandem sensors, as the newer generation indicators are brighter and have larger dynamic ranges compared to GCaMP3[11] (Figure 2). GCaMP3, GCaMP6s, and GCaMP6f were linked to mCherry *via* either an ER/K α-helix or the DELTA sequence (Figure 2A). In order to measure dynamic range (DR)—defined as $(R_{max} - R_{min})/R_{min}$—of the purified tandem sensors, the emission spectra of GCaMP3, GCaMP6s, and GCaMP6f were measured in 1 mM $CaCl_2$ or 1 mM EGTA. The emission spectrum of mCherry in each tandem sensor was also measured. Then, for each sensor the emission spectrum of the GCaMP variant was divided by the peak emission intensity of mCherry at 608 nm, to normalize for protein concentrations. R_{max} and R_{min} values were defined as the ratios of the peaks of GCaMP normalized to mCherry in 1 mM $CaCl_2$ (Figure 2B–D) or 1 mM EGTA (Figure 2E–G), respectively.

Consistent with the data from Figure 1, R_{max} and R_{min} values of 3-ER/K, 6s-ER/K, and 6f-ER/K sensors were significantly larger than those of 3-DELTA, 6s-DELTA, and 6f-DELTA sensors (Figure 2H,I). R_{max} values of 3-ER/K, 6s-ER/K, and 6f-ER/K were increased by 52%, 33%, 125% compared to those of DELTA sensors. R_{min} values of 3-ER/K, 6s-ER/K, and 6f-ER/K were increased by 32%, 31%, 90% compared to those of DELTA sensors. In the absence of FRET, the ratios of GCaMP over mCherry were significantly larger at maximum and minimum calcium concentrations. Note that preventing FRET is especially advantageous for GCaMP6s and GCaMP6f, as basal fluorescence intensities of GCaMP6s and GCaMP6f are dimmer than that of GCaMP3. The DR of 3-ER/K and 6f-ER/K was 16% and 26% larger than that of the corresponding DELTA sensors, but 6s-ER/K showed a −2% change in DR. Taken together, not only were the peak ratios of ER/K sensors at maximum and minimum calcium levels higher but also the DR of 3-ER/K and 6f-ER/K was improved.

The pH and magnesium sensitivity of GCaMP-R variants were also investigated (Figure S1). GCaMP fluorescence was sensitive to pH, the intensity increasing with increasing pH both in the presence and absence of calcium, but mCherry fluorescence was not affected. Neither GCaMPs nor mCherry showed much sensitivity to magnesium concentrations. The net effect was that increasing pH reduced the dynamic range of GCaMP-R variants. Users should, therefore, be aware that changes in cell pH may affect accuracy of calcium measurements with this probe.

ER/K α-Helix Linker Increases GCaMP Signals *in Cellulo*

AtT20 cells were chosen to test the function of the tandem sensors, as they express voltage-gated calcium channels and show spontaneous electrical spiking activity.[22] The ratios of GCaMP over mCherry intensity were obtained by direct excitation (at 473 and 561 nm, respectively) of the fluorophores. As shown in Figure 3, 100 mM KCl solution was applied for a 10-s period to AtT20 cells expressing the tandem sensors to evoke depolarization-induced calcium influx. Even before KCl application, approximately 35% of the cells showed random calcium fluctuations. Consistent with the in vitro experiments, the peak ratios of 3-ER/K, 6s-ER/K, and 6f-ER/K in response to KCl were significantly larger than those of 3-DELTA, 6s-DELTA, and 6f-DELTA sensors (Figure 3A–C). In order to assay for FRET, mCherry emission obtained when exciting only at the GCaMP excitation wavelength (473 nm) was measured simultaneously with GCaMP emission, using an optical splitter (Figure 3D). Unlike ER/K sensors, 3-DELTA, 6s-DELTA, and 6f-DELTA exhibited significantly increased mCherry intensity upon high KCl application, implying that FRET occurred in DELTA sensors.

In order to estimate the dynamic range of the tandem sensors, the cells were sequentially challenged with 20 mM EGTA-buffered zero calcium solution (R_{min}) and 15 mM $CaCl_2$ solution (R_{max}) after the KCl stimulation (Figure 3A–C). To disable the cell's intrinsic ability to regulate free calcium concentrations, 10 μM ionomycin, 5 μM thapsigargin, and 10 μM CCCP were added into the R_{min} and R_{max} solutions.[7,23] Random calcium fluctuations disappeared in the R_{min} solution. R_{min} values were averaged over a 5-s period immediately before the application of R_{max} solution. R_{max} values were averaged over a 5-s period during which the ratios were at a maximum. Corroborating the data obtained with purified protein

in vitro, R_{min} and R_{max} values of ER/K sensors expressed in cells were significantly larger than those of DELTA sensors expressed in cells (Figure 3E,F). R_{max} values of 3-ER/K, 6s-ER/K, and 6f-ER/K were increased by 35%, 22%, and 48% compared to those of DELTA sensors. R_{min} values of 3-ER/K, 6s-ER/K, and 6f-ER/K were changed by 36%, 0%, and 18% compared to those of DELTA sensors. FRET ratios were significantly larger in 3-DELTA, 6s-DELTA, and 6f-DELTA sensors, but not in ER/K sensors (Figure 3G,H). Compared with DELTA sensors, the dynamic ranges of 6s-ER/K and 6f-ER/K were increased by 22% and 23%, respectively, but only 2% in 3-ER/K. The normalized fluorescence intensities of the data set in Figure 3 is shown in Figure S2.

Expression of GCaMP-R Variants in Live Tissues

Next, we tested 6s-ER/K (renamed "GCaMP-R-6s") expressed in intact tissues to detect the change of calcium levels. First we used developing chicken neural tubes (Figure 4). As shown in Figure 4A, expression driven by the cytomegalovirus (CMV) promoter leads to differing levels of sensor expression in developing neurons, as indicated by the varying mCherry fluorescence intensities. GCaMP6s and mCherry fluorescence were localized to the cytoplasm. For region of interest (ROI) analysis, regions in the cytoplasm of four cells were selected (ROI1–4, Figure 4A). The averages of mCherry intensity in three cells indicated with arrowheads were close to maximum value of image bit depth, so they were excluded for ROI analysis. When 100 mM KCl solution was applied to the neurons, the GCaMP6s signal dramatically increased (Movies S1 and S2). Note that 100 mM KCl induced tissue movement during recordings, so the mCherry intensity might appear to change slightly over time (Figure 4E).

The function of GCaMP-R-6s was also tested in retinal slices from mouse retina wherein rod photoreceptors were transduced with a recombinant, serotype 2-based adeno-associated virus-rAAV2 (quad Y-F),[24] which had been optimized for transduction of photoreceptor cells (Figure 5). In order to increase the inset capacity of the viral vector, instead of the CMV immediate-early enhancer/chicken ß-actin (CBA) promoter, we used the smCBA promoter (a truncated version of CBA)[25] to drive GCaMP-R-6s expression. The photoreceptor cell layer is shown in the cross section of the retina (Figure 5A), with the outer segment (OS) arranged to the left, followed by the inner segment (IS), cell body (CB), and synaptic compartments (Syn) at the right. The highly structured layering of the retina allowed us to visualize the calcium transients, as well as the relative calcium levels within these compartments. In some cells, bright mCherry puncta not associated with GCaMP6 fluorescence were observed (Figure 5C, large arrows). To see whether these mCherry puncta reflect proteolysis that separated mCherry fluorescence from that of GCaMP6s, Western blots were performed on retinal homogenates from control and rAAV2 (quad Y–F)-transduced retinas using antibodies against the amino and carboxyl termini of the fusion protein (Figure S5). No truncated products were observed, suggesting that protein aggregation suppressed fluorescence of GCaMP6s but not that of mCherry.

In the dark, sodium and calcium ions flow into the rod photoreceptor outer segment through the open cGMP-gated channels. Thus, in the dark-adapted state, the intracellular calcium concentration is high and measured to be 250 ± 20 nM in the mouse rod outer segment.[26] At

the rod synapse, calcium ions enter through the voltage-gated calcium channels (VGCCs), supporting a tonic release of the neurotransmitter, glutamate. Light triggers a G-protein-mediated signaling cascade, which results in cGMP hydrolysis and closure of the cGMP-gated channels, leading to a fall in calcium concentration in the outer segment to 23 ± 2 nM.[26] In addition, the cell hyperpolarizes, causing closure of VGCCs, and calcium entry at the synapse declines. Therefore, light exposure lowers calcium levels at the outer segment and synaptic compartments. As expected, the fluorescence intensity of GCaMP6s was low in the majority of labeled rods in all compartments because the retinal slices were prepared under room light (Figure 5B, 0 s). The mCherry fluorescence signal was used to locate labeled cells (Figure 5C). Application of KCl caused calcium entry at the synapse (Figure 5B, 169 s, Movie S3). Increased GCaMP6s fluorescence then travels toward the cell body (Figure 5B, 172 –192 s). After 172 s, the tissue moved out of the focal plane in response to KCl application.

The increase in calcium level in the synaptic (ROI1) and cell body compartments (ROI2) was further analyzed by calculating the ratio of the intensity of GCaMP6s and mCherry as a function of time (Figure 5D). These values were plotted and shown in Figure 5E–G, where it can be seen that the GCaMP6s fluorescence increased while mCherry fluorescence remained unchanged following KCl application. In some instances, where the entire cell can be observed within the focal plane, GCaMP6s fluorescence change continued to travel from the cell body toward the inner segment. Interestingly, the calcium transient wave did not cross from the inner to the outer segment compartment following KCl application (Movies S3 and S4). To confirm this observation, six cells were further analyzed (Figure 5H). The fluorescence intensity of GCaMP6s (Figure 5I) and mCherry (Figure 5J) were quantified at the outer segment compartment and plotted as a function of time. Five out of six ROIs positioned at the inner and outer segments of rod photoreceptors did not respond to KCl (Figure 5K). These observations are consistent with previous studies that show compartmentalization of calcium handling in different cell compartments within vertebrate rod photoreceptor cells.[27] Together, these results demonstrate the suitability of the GCaMP-R-6s for not only the detection of calcium transients but, more importantly, the relative calcium levels in different subcellular compartments of the mammalian rod photoreceptor cell.

Calcium Calibration

The set of GCaMP-R variants was expressed in AtT20 cells. In order to control calcium concentration, cells were incubated in a cocktail containing calcium buffered to a defined level, the calcium ionophore ionomycin, thapsigargin (to block calcium uptake into ER calcium stores), and the protonophore CCCP (to indirectly block calcium uptake by collapsing the mitochondria membrane potential and thereby halting generation of ATP, which would otherwise energize calcium pumps).[7,23] The defined free calcium concentrations were 0 nM, 50 nM, 100 nM, 223 nM, 447 nM, 1.34 μM, and 15 mM (Figure 6D). Normalized ratios were plotted against the seven free calcium concentrations and fitted with the Hill equation (Figure 6 legend) to estimate the apparent dissociation constant (K_D) and Hill coefficient (n). The K_D of GCaMP-R-3, GCaMP-R-6s, and GCaMP-R-6f was 578 ± 22 nM, 258 ± 11 nM, and 722 ± 33 nM, respectively. The Hill coefficient of GCaMP-R-3,

GCaMP-R-6s, and GCaMP-R-6f was 2.06 ± 0.1, 2.05 ± 0.2, and 2.07 ± 0.1, respectively. Unperturbed AtT20 cells exhibited various shapes of calcium signals, and approximately 35% of cells exhibited spontaneous calcium elevations during 400 s recordings (Figure 6A–C). Three representative cells expressing the similar mCherry fluorescence intensity (and, therefore, similar GCaMP calcium buffering) were chosen in order to estimate free calcium concentrations (Figure 6A–C). The ratios were converted into free calcium concentrations using the equation (1) derived by Palmer and Tsien[28] (Figure 6 legend and method). In order to compare calcium levels among GCaMP-R variants, the lowest calcium levels at interspike intervals (ISIs) during the recordings were measured (Figure 6E). Unlike GCaMP-R-3 and GCaMP-R-6f, high affinity GCaMP-R-6s sensors showed significantly lower calcium levels.

Conclusion

Dual fluorescent protein reporters for ratio-metric measurements are not new, but previous generations have suffered from certain drawbacks. For example, constructs have been designed with the fluorophores separated by either 2A fusion peptides or internal ribosome entry sites (IRESs), leading to coexpression of GCaMP and red fluorescence protein in tissues.[29,30] Constructs using a 2A peptide are translated to yield two proteins at equimolar concentrations; however, depending upon the type of 2A peptide (P2A, T2A, E2A, F2A) and the tissue that is targeted, different cleavage efficiency has been observed.[31] It is also possible that cleavage efficiency differs among cells even within one population. Moreover, the cleavage occurs cotranslationally, and uncleaved products (10%) are not able to undergo post-translational cleavage.[32] As shown in our study, if cleavage were not to occur, the 2A peptide linking the GCaMP and mCherry would be short enough (18–22 amino acid residues) to allow FRET, thereby reducing the GCaMP/mCherry ratio. Preventing FRET at low calcium level is particularly important in applications using GCaMP-R-6s and GCaMP-R-6f, because the ratio of GCaMP-R-6s and -6f at zero calcium concentration is barely above the background and 39% or 37% smaller than that of GCaMP-R-3, respectively. The elimination of FRET by introducing the ER/K helix serves to increase GCaMP fluorescence above the background, which improves the SNR.

A major disadvantage of using an IRES is that the upstream gene is translated at a much higher rate (90%) than the downstream gene,[33] and once expressed, the separate proteins may undergo degradation at different rates. Another complication with the IRES constructs is differential localization of the two fluorescent proteins (Figure S3). We found that in HEK293T cells, mCherry was found both in the nuclei and the cytoplasm, whereas GCaMP3 was located in the cytoplasm. Moreover, the ratio of fluorescence intensities with the IRES construct showed a far higher coefficient of variation than did the ratio with the tandem constructs (Figure S4). Taken together, constructs based on 2A or IRES cannot be counted on for ratiometric measurements at “anytime” and “anywhere” within individual cells.

Although expression of GCaMP-Rs was relatively homogeneous within most cell compartments, we did observe possible aggregation of mCherry in rod photoreceptors when the sensors were overexpressed (Figure 5C, large arrowheads; see Figure S5, Western blots of retinal homogenate with rAAV2 (quad Y–F)-injected retina (see also Movie S3)).

Overabundance is also a concern for any protein that buffers calcium. All exogenously introduced calcium indicators may alter a cell's intrinsic calcium signaling by altering the total calcium buffering capacity. Thus, one must carefully balance the need for maximum signal output versus the need for minimal disturbance of the endogenous calcium buffering system.[34] The K_D of purified GCaMP variants measured *in vitro* varies from nM to 447 nM,[11] which is appropriate for measuring physiological calcium levels from about 0.1 μM to 10 μM. However, high affinity sensors like GCaMP-R-6s may seriously distort the rise and decay kinetics, as well as peak amplitude, of calcium signals, depending on the level of expression (Figure 4B large arrowheads indicate the cells expressing higher sensor concentrations and long lasting calcium levels even after washout of KCl). When overexpression is a concern, it may be necessary to use a weaker protein expression promoter.

Another possible concern is the different photobleaching rates of the GCaMP and mCherry fluorophores. The photobleaching rate of mCherry under continuous arc lamp illumination ($t_{1/2}$ = 96 s) is about 1.8 times faster than that of EGFP ($t_{1/2}$ = 174 s),[35] which could pose a potential problem for quantitative ratiometric measurements. In our experience, however, bleaching of GCaMP variants and mCherry was reduced to almost negligible over the time period of a typical experiment (400 s), by reducing illumination intensity with neutral density filters, gating the illumination solely to periods of image acquisition, and using a highly sensitive EMCCD camera.

In summary, GCaMP-R sensors presented here offer the advantage of high signal-to-noise ratiometric calcium imaging and will allow pixelwise imaging for specific cells and specific subcellular locations. The GCaMP-R sensors will readily accommodate improved GCaMP variants, as well as alternatives to mCherry protein serving as the calcium-independent fluorescent reference protein,[36] and thus should continue to improve over time. The GCaMP-Rs presented here will be able to not only report the occurrence of calcium spiking activity but also provide estimates of maintained or basal calcium levels. As demonstrated here, when expressing GCaMP-Rs in retinal rod photoreceptors, GCaMP-Rs can facilitate observations of calcium handling in different subcellular compartments in the same cell and thus may facilitate studying how calcium dynamics in one cellular compartment may affect calcium dynamics in other compartments. GCaMP-Rs offer a tool to study how altered basal calcium concentration and calcium homeostasis may play a role in such pathological processes as retinal degeneration.[37]

Acknowledgments

We thank Y. Yao and M. Ritt for technical assistance in making the bicistronic and tandem constructs. We thank S. Vogel, L. Cohen, and A Weitz for critical feedback on the manuscript. We thank C.-Y. Yeh, who kindly shared the intensity modulated ratiometric image display analysis routine. This research was supported by NIH grant R01 GM85791 to RH. Chow, R01 EY022931 (to J. Weiland and R.H. Chow), EY12155, EY027193 (to J. Chen), 1DP2 CA186752-01 (to S. Sivaramakrishnan), R01 AR47364, and AR60306 (to C.-M. Chuong).

References

1. Tsien RY. New calcium indicators and buffers with high selectivity against magnesium and protons: design, synthesis, and properties of prototype structures. Biochemistry. 1980; 19:2396–2404. [PubMed: 6770893]
2. Grynkiewicz G, Poenie M, Tsien RY. A new generation of Ca^{2+} indicators with greatly improved fluorescence properties. J. Biol. Chem. 1985; 260:3440–3450. [PubMed: 3838314]
3. Behrend MR, Ahuja AK, Humayun MS, Weiland JD, Chow RH. Selective labeling of retinal ganglion cells with calcium indicators by retrograde loading in vitro. J. Neurosci. Methods. 2009; 179:166–172. [PubMed: 19428523]
4. Andermann ML, Kerlin AM, Reid RC. Chronic cellular imaging of mouse visual cortex during operant behavior and passive viewing. Front. Cell. Neurosci. 2010; 4:3. [PubMed: 20407583]
5. Chhatwal JP, Hammack SE, Jasnow AM, Rainnie DG, Ressler KJ. Identification of cell-type-specific promoters within the brain using lentiviral vectors. Gene Ther. 2007; 14:575–583. [PubMed: 17235291]
6. Mao T, O'Connor DH, Scheuss V, Nakai J, Svoboda K. Characterization and subcellular targeting of GCaMP-type genetically-encoded calcium indicators. PLoS One. 2008; 3:e1796. [PubMed: 18350138]
7. Sztretye M, Yi J, Figueroa L, Zhou J, Royer L, Ríos E. D4cpv-calsequestrin: a sensitive ratiometric biosensor accurately targeted to the calcium store of skeletal muscle. J. Gen. Physiol. 2011; 138:211–229. [PubMed: 21788610]
8. Akerboom J, Chen TW, Wardill TJ, Tian L, Marvin JS, Mutlu S, Calderon NC, Esposti F, Borghuis BG, Sun XR, Gordus A, Orger MB, Portugues R, Engert F, Macklin JJ, Filosa A, Aggarwal A, Kerr RA, Takagi R, Kracun S, Shigetomi E, Khakh BS, Baier H, Lagnado L, Wang SS, Bargmann CI, Kimmel BE, Jayaraman V, Svoboda K, Kim DS, Schreiter ER, Looger LL. Optimization of a GCaMP calcium indicator for neural activity imaging. J. Neurosci. 2012; 32:13819–13840. [PubMed: 23035093]
9. Zariwala HA, Borghuis BG, Hoogland TM, Madisen L, Tian L, De Zeeuw CI, Zeng H, Looger LL, Svoboda K, Chen TW. A Cre-dependent GCaMP3 reporter mouse for neuronal imaging in vivo. J. Neurosci. 2012; 32:3131–3141. [PubMed: 22378886]
10. Tian L, Hires SA, Mao T, Huber D, Chiappe ME, Chalasani SH, Petreanu L, Akerboom J, McKinney SA, Schreiter ER, Bargmann CI, Jayaraman V, Svoboda K, Looger LL. Imaging neural activity in worms, flies and mice with improved GCaMP calcium indicators. Nat. Methods. 2009; 6:875–881. [PubMed: 19898485]
11. Chen TW, Wardill TJ, Sun Y, Pulver SR, Renninger SL, Baohan A, Schreiter ER, Kerr RA, Orger MB, Jayaraman V, Looger LL, Svoboda K, Kim DS. Ultrasensitive fluorescent proteins for imaging neuronal activity. Nature. 2013; 499:295–300. [PubMed: 23868258]
12. Zhao Y, Araki S, Wu J, Teramoto T, Chang YF, Nakano M, Abdelfattah AS, Fujiwara M, Ishihara T, Nagai T, Campbell RE. An expanded palette of genetically encoded Ca^{2+} indicators. Science. 2011; 333:1888–1891. [PubMed: 21903779]
13. Wu J, Abdelfattah AS, Miraucourt LS, Kutsarova E, Ruangkittisakul A, Zhou H, Ballanyi K, Wicks G, Drobizhev M, Rebane A, Ruthazer ES, Campbell RE. A long Stokes shift red fluorescent Ca^{2+} indicator protein for two-photon and ratiometric imaging. Nat. Commun. 2014; 5:5262. [PubMed: 25358432]
14. Palmer AE, Giacomello M, Kortemme T, Hires SA, Lev-Ram V, Baker D, Tsien RY. Ca^{2+} indicators based on computationally redesigned calmodulin-peptide pairs. Chem. Biol. 2006; 13:521–530. [PubMed: 16720273]
15. Mank M, Santos AF, Direnberger S, Mrsic-Flogel TD, Hofer SB, Stein V, Hendel T, Reiff DF, Levelt C, Borst A, Bonhoeffer T, Hubener M, Griesbeck O. A genetically encoded calcium indicator for chronic in vivo two-photon imaging. Nat. Methods. 2008; 5:805–811. [PubMed: 19160515]
16. Thestrup T, Litzlbauer J, Bartholomaus I, Mues M, Russo L, Dana H, Kovalchuk Y, Liang Y, Kalamakis G, Laukat Y, Becker S, Witte G, Geiger A, Allen T, Rome LC, Chen TW, Kim DS, Garaschuk O, Griesinger C, Griesbeck O. Optimized ratiometric calcium sensors for functional in

vivo imaging of neurons and T lymphocytes. Nat. Methods. 2014; 11:175–182. [PubMed: 24390440]

17. Sun XR, Badura A, Pacheco DA, Lynch LA, Schneider ER, Taylor MP, Hogue IB, Enquist LW, Murthy M, Wang SS. Fast GCaMPs for improved tracking of neuronal activity. Nat. Commun. 2013; 4:2170. [PubMed: 23863808]
18. Badura A, Sun XR, Giovannucci A, Lynch LA, Wang SS. Fast calcium sensor proteins for monitoring neural activity. Neurophotonics. 2014; 1:025008. [PubMed: 25558464]
19. Sivaramakrishnan S, Spudich JA. Systematic control of protein interaction using a modular ER/K α-helix linker. Proc. Natl. Acad. Sci. U. S. A. 2011; 108:20467–20472. [PubMed: 22123984]
20. Swanson CJ, Sivaramakrishnan S. Harnessing the unique structural properties of isolated α-helices. J. Biol. Chem. 2014; 289:25460–25467. [PubMed: 25059657]
21. Day RN, Davidson MW. The fluorescent protein palette: tools for cellular imaging. Chem. Soc. Rev. 2009; 38:2887–2921. [PubMed: 19771335]
22. Adler M, Wong BS, Sabol SL, Busis N, Jackson MB, Weight FF. Action potentials and membrane ion channels in clonal anterior pituitary cells. Proc. Natl. Acad. Sci. U. S. A. 1983; 80:2086–2090. [PubMed: 6300893]
23. Chen L, Koh DS, Hille B. Dynamics of calcium clearance in mouse pancreatic beta-cells. Diabetes. 2003; 52:1723–1731. [PubMed: 12829639]
24. Zolotukhin S, Potter M, Zolotukhin I, Sakai Y, Loiler S, Fraites TJ Jr, Chiodo VA, Phillipsberg T, Muzyczka N, Hauswirth WW, Flotte TR, Byrne BJ, Snyder RO. Production and purification of serotype 1, 2, and 5 recombinant adeno-associated viral vectors. Methods. 2002; 28:158–167. [PubMed: 12413414]
25. Flannery JG, Zolotukhin S, Vaquero MI, LaVail MM, Muzyczka N, Hauswirth WW. Efficient photoreceptor-targeted gene expression in vivo by recombinant adeno-associated virus. Proc. Natl. Acad. Sci. U. S. A. 1997; 94:6916–6921. [PubMed: 9192666]
26. Woodruff ML, Sampath AP, Matthews HR, Krasnoperova NV, Lem J, Fain GL. Measurement of cytoplasmic calcium concentration in the rods of wild-type and transducin knock-out mice. J. Physiol. 2002; 542:843–854. [PubMed: 12154183]
27. Krizaj D, Copenhagen DR. Compartmentalization of calcium extrusion mechanisms in the outer and inner segments of photoreceptors. Neuron. 1998; 21:249–256. [PubMed: 9697868]
28. Palmer AE, Tsien RY. Measuring calcium signaling using genetically targetable fluorescent indicators. Nat. Protoc. 2006; 1:1057–1065. [PubMed: 17406387]
29. Rose T, Jaepel J, Hubener M, Bonhoeffer T. Cell-specific restoration of stimulus preference after monocular deprivation in the visual cortex. Science. 2016; 352:1319–1322. [PubMed: 27284193]
30. Gee J-M, Smith N-A, Fernandez F-R, Economo M-N, Brunert D, Rothermel M, Morris S-C, Talbot A, Palumbos S, Ichida J-M, Shepherd J-D, West P-J, Wachowiak M, Capecchi M-R, Wilcox K-S, White J-A, Tvrdik P. Imaging activity in neurons and glia with a Polr2a–based and cre-dependent GCaMP5G–IRES-tdTomato reporter mouse. Neuron. 2014; 83:1058–1072. [PubMed: 25155958]
31. Kim J-H, Lee S-R, Li L-H, Park H-J, Park J-H, Lee K-Y, Kim M-K, Shin B-A, Choi S-Y. High cleavage efficiency of a 2A peptide derived from porcine teschovirus-1 in human cell lines, zebrafish and mice. PLoS One. 2011; 6:e18556. [PubMed: 21602908]
32. de Felipe P, Luke G-A, Hughes L-E, Gani D, Halpin C, Ryan M-D. E unum pluribus: multiple proteins from a self-processing polyprotein. Trends Biotechnol. 2006; 24:68–675. [PubMed: 16380176]
33. de Felipe P. Polycistronic viral vectors. Curr. Gene Ther. 2002; 2:355–378. [PubMed: 12189721]
34. Rose T, Goltstein PM, Portugues R, Griesbeck O. Putting a finishing touch on GECIs. Front. Mol. Neurosci. 2014; 7:88. [PubMed: 25477779]
35. Shaner NC, Lin MZ, McKeown MR, Steinbach PA, Hazelwood KL, Davidson MW, Tsien RY. Improving the photostability of bright monomeric orange and red fluorescent proteins. Nat. Methods. 2008; 5:545–551. [PubMed: 18454154]
36. Chu J, Oh Y, Sens A, Ataie N, Dana H, Macklin J-J, Laviv T, Welf E-S, Dean K-M, Zhang F, Kim B-B, Tang C-T, Hu M, Baird M-A, Davidson M-W, Kay M-A, Fiolka R, Yasuda R, Kim D-S, Ng H-L, Lin M-Z. A bright cyan-excitable orange fluorescent protein facilitates dual-emission

microscopy and enhances bioluminescence imaging in vivo. Nat. Biotechnol. 2016; 34:760–767. [PubMed: 27240196]

37. Fain GL. Why photoreceptors die (and why they don't). BioEssays. 2006; 28:344–354. [PubMed: 16547945]

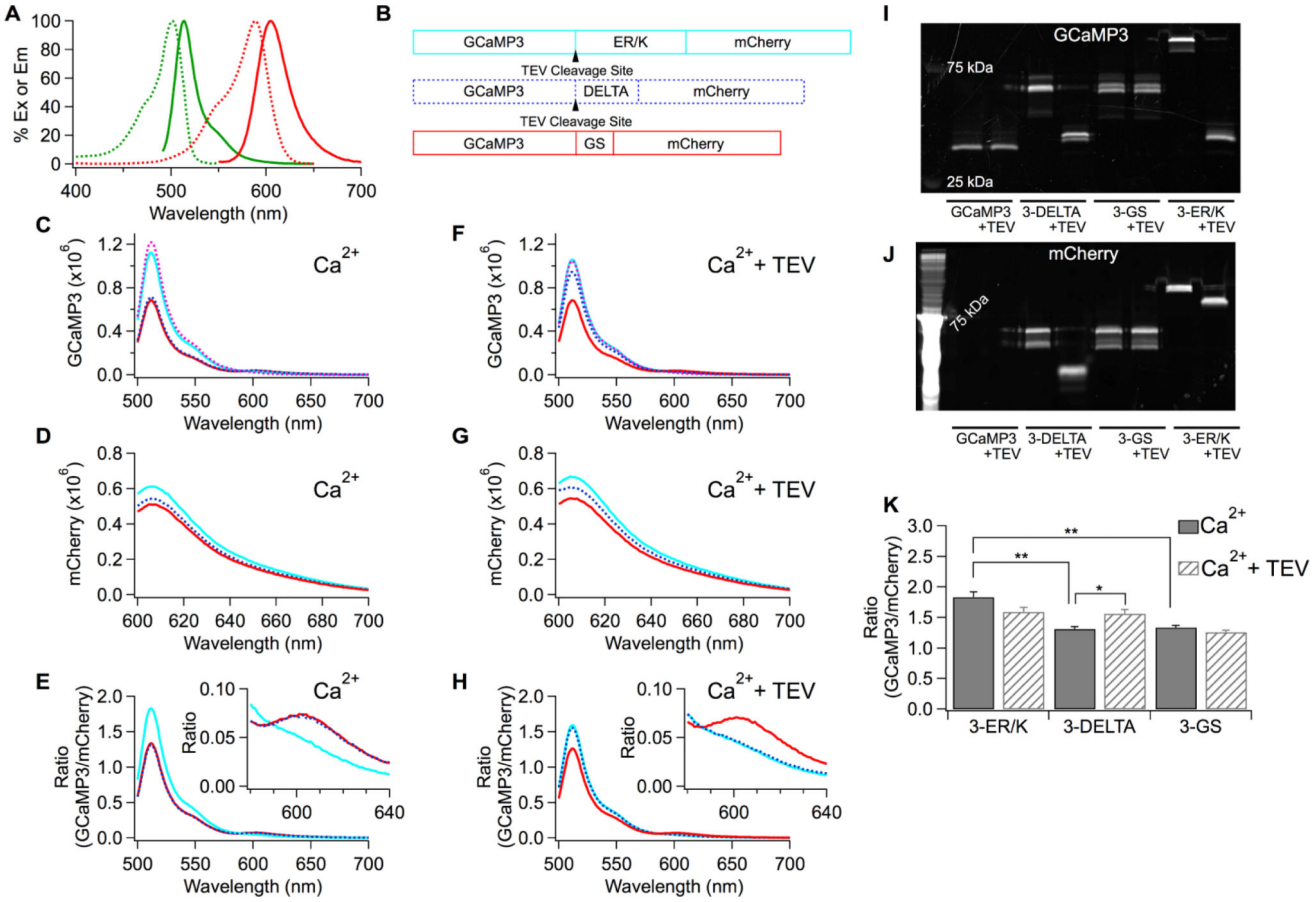

Figure 1.

Prevention of FRET between GCaMP3 and mCherry by ER/K helix. (A) Excitation (dash) and emission (solid) spectra of GCaMP3 (green) and mCherry (red) proteins. (B) Schematic drawing of tandem sensors with the different linkers. (C–H) Emission spectra of the tandem GCaMP3 and mCherry proteins in $CaCl_2$ solution without TEV protease (C,D,E) or with TEV protease (F,G,H). Spectra of GCaMP3 alone (dashed pink) added to compare with those of the tandem sensors in panels C and F. (E,H) The peak intensity at 608 nm of the mCherry emission spectrum (D,G) was used to normalize the GCaMP3 emission spectrum denoted as Ratio (GCaMP3/mCherry) in each tandem sensor. Insets zoomed in on the spectra around 600 nm. (I,J) The protein samples used for obtaining the emission spectra (C–H) were run on a gel and visualized by exciting either GCaMP3 (I) or mCherry (J) to confirm the cleavage of GCaMP3 from mCherry. (K) Average peak ratios at 511 nm obtained from (E,H). Mean ± SEM (**$p < 0.01$, *$p < 0.05$, $n = 3$ for each condition).

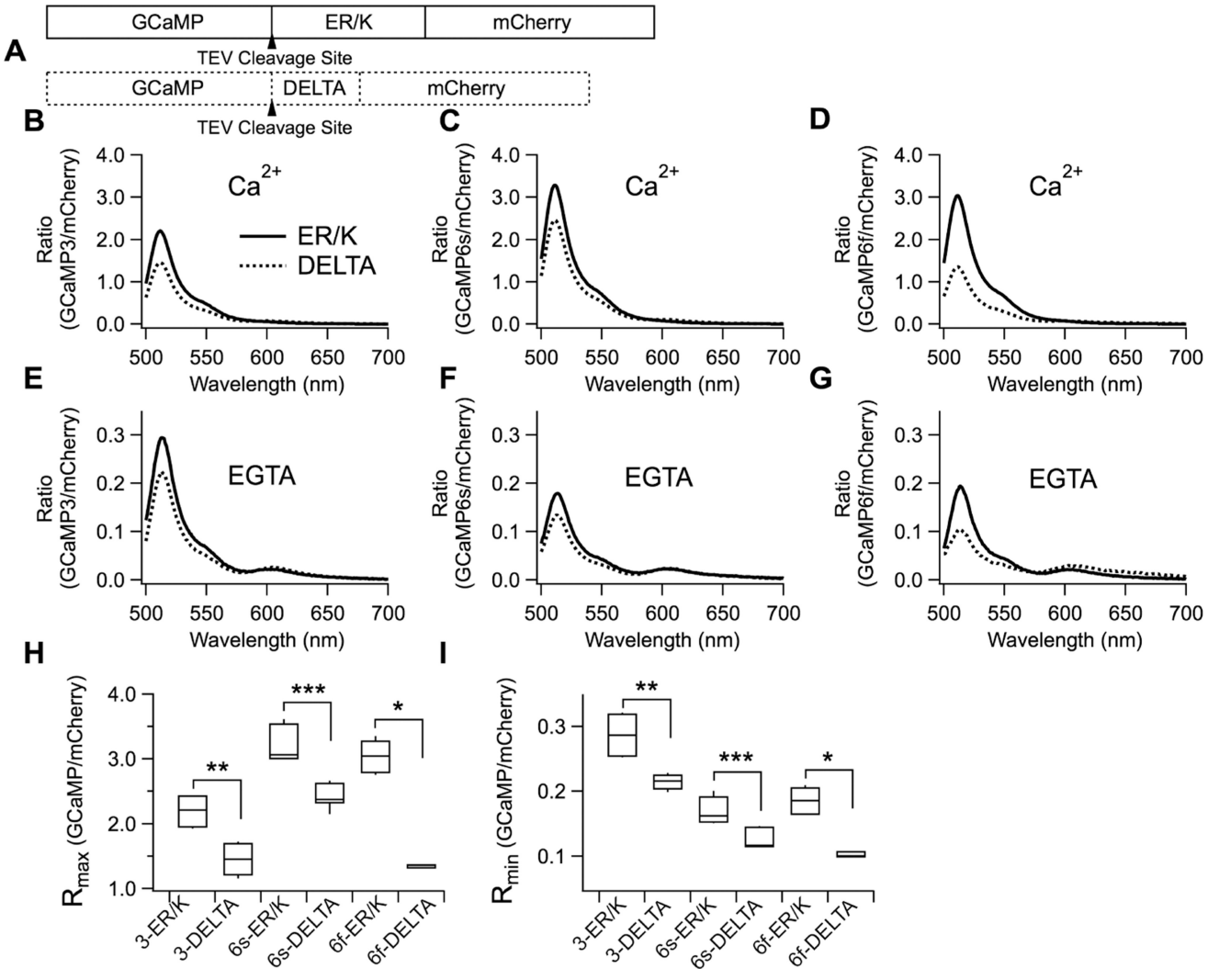

Figure 2.

Increase in signals of GCaMP variants at high and zero calcium solutions *in vitro* by ER/K linker. (A) Schematic drawing of ER/K and DELTA sensors. (B–G) GCaMP emission spectra normalized to peak emission intensity of mCherry in $CaCl_2$ solution (B,C,D) or EGTA (E,F,G). (B,E) 3-ER/K ($n = 6$) and 3-DELTA ($n = 6$). (C,F) 6s-ER/K ($n = 9$) and 6s-DELTA ($n = 9$). (D,G) 6f-ER/K ($n = 6$) and 6f-DELTA ($n = 3$). (H,I) R_{max} and R_{min} were defined as the peak ratios of the normalized GCaMP spectra in $CaCl_2$ solution or EGTA, respectively. Mean ± SEM (***$p < 0.001$, **$p < 0.01$, *$p < 0.05$).

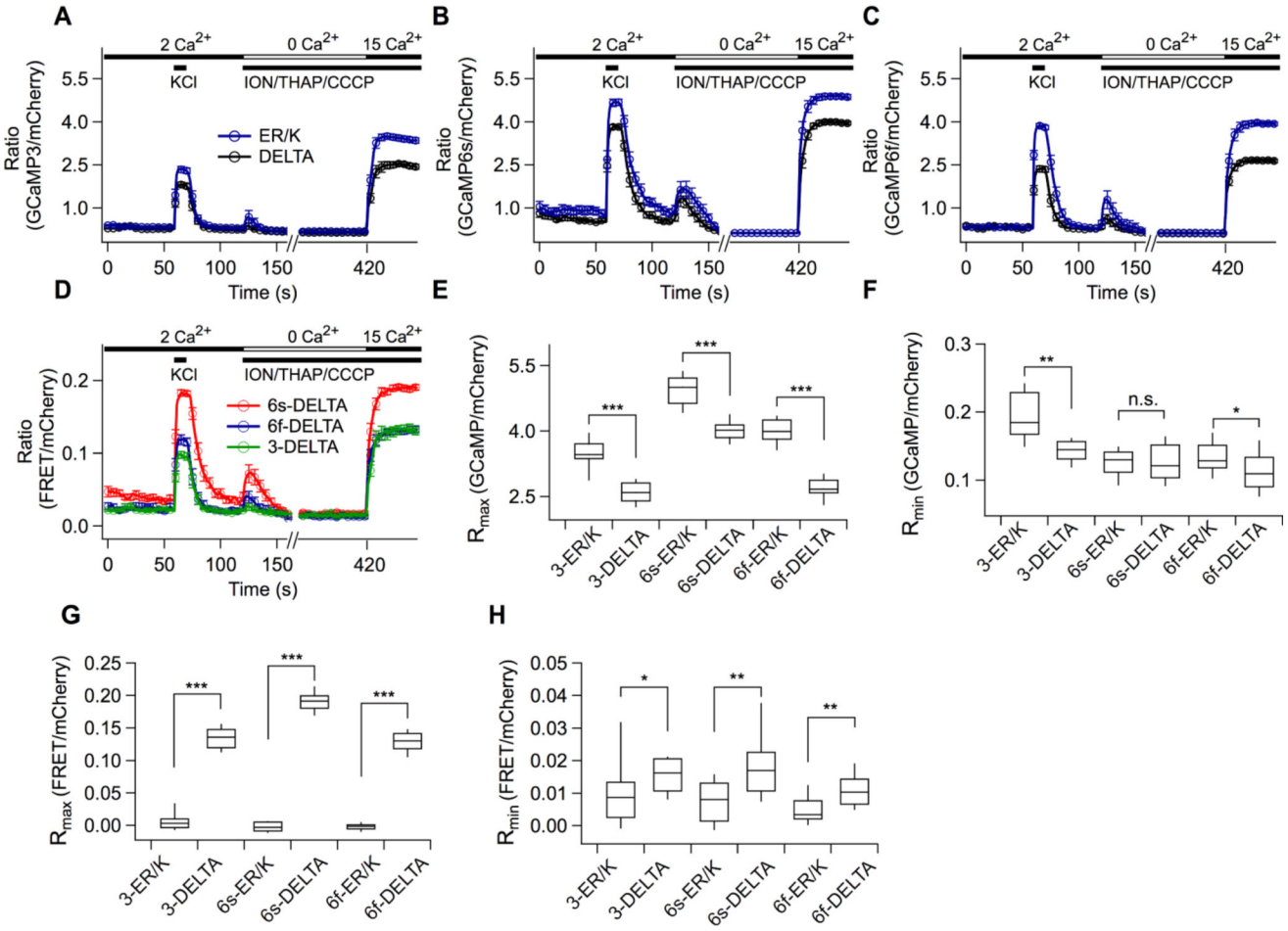

Figure 3.

Increased signals of GCaMP variants in high and zero calcium solutions in AtT20 cells by ER/K linker. (A–D) Three types of emission intensities at excitation wavelength 473 or 561 nm were obtained: (1) intensity for direct excitation of GCaMP, (2) intensity for direct excitation of mCherry, (3) intensity for GCaMP excitation-mCherry emission denoted as FRET. GCaMP and mCherry fluorescence were separated using an optical splitter. Averaged ratios for direct excitation of GCaMP over mCherry were plotted against time (A, 3-ER/K, n = 9; B, 6s-ER/K, n = 23; C, 6f-ER/K, n = 20), while GCaMP-induced mCherry fluorescence (FRET) for direct GCaMP excitation was normalized to mCherry fluorescence at direct mCherry excitation (D, 3-DELTA, n = 9; 6s-DELTA, n = 20; 6f-DELTA, n = 15). A custom-built local perfusion system was located right next to a field of view, leading to a change of each test solution with a time constant of ~100 ms. The cells were sequentially applied with high KCl, R_{min}, and R_{max} solutions. (E,F) R_{max} and R_{min} values of the ER/K and DELTA sensors obtained from A-C. (G,H) R_{max} and R_{min} values obtained from D. Mean ± SEM (***$p < 0.001$, **$p < 0.01$, *$p < 0.05$).

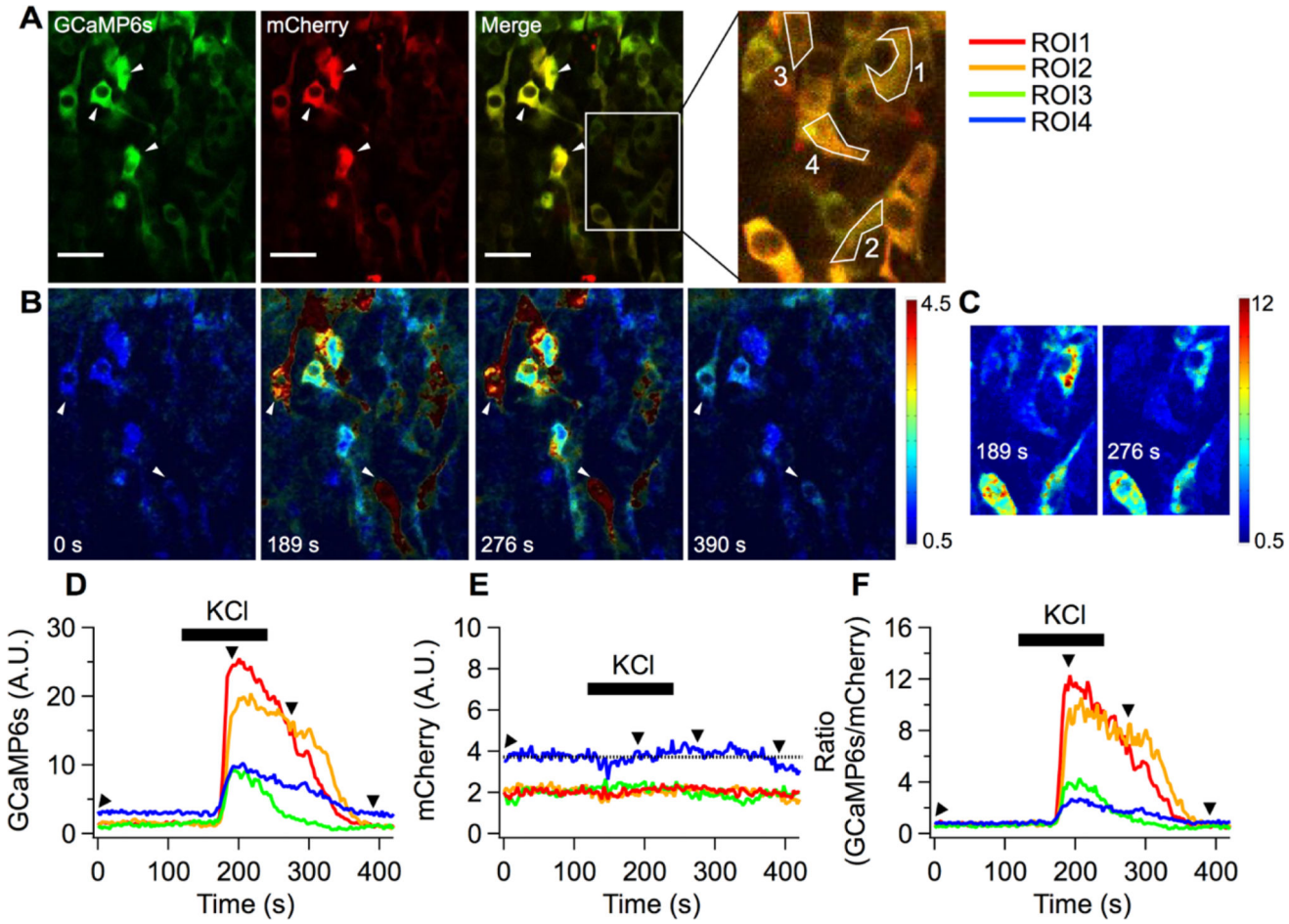

Figure 4.

Functional GCaMP-R-6s expressed in developing chicken neural tube. (A) Average images of GCaMP6s and mCherry obtained in Ringer's solution. Four regions of interest (ROI1–4) located at cell bodies were chosen for calculating mean fluorescence intensity of GCaMP6s and mCherry. Scale bars, 25 μm. (B) KCl solution was applied to the neural tube to evoke depolarization-induced calcium influx during a time-series recording. Due to the bath perfusion configuration, KCl responses were delayed by ~50 s. Pseudo-color ratiometric images were displayed to estimate relative calcium elevations in cells expressing varying levels of the sensor. Four images were corresponding to time points shown in D, GCaMP6s; E, mCherry; and F, ratio of GCaMP6s over mCherry as black arrowheads. (C) Subset images including the four ROIs at two different time points shown in F were chosen to display the full range of ratios.

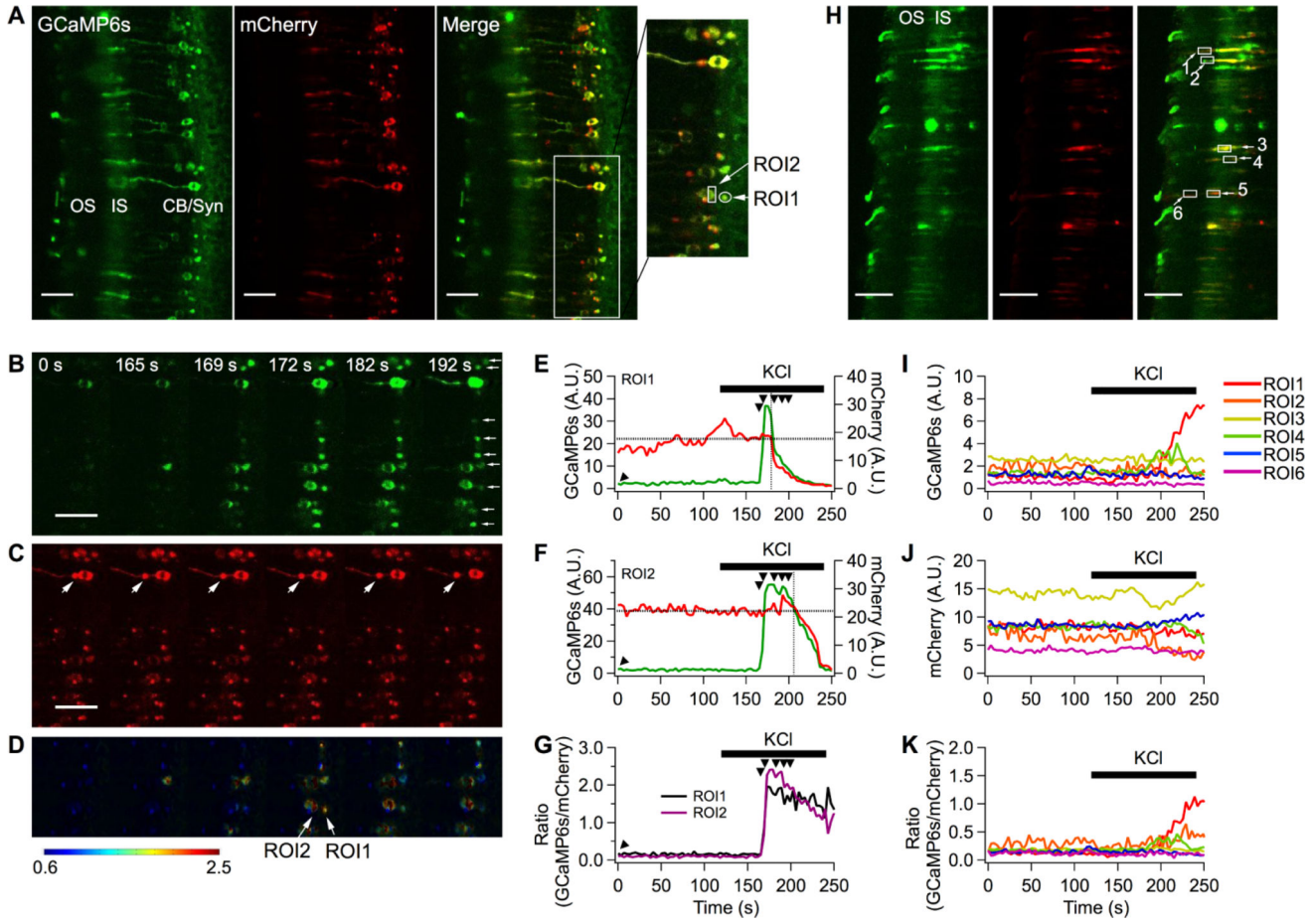

Figure 5.

Calcium measurements for different compartments in mouse retina rod photoreceptors. (A) Average images of GCaMP6s and mCherry obtained in Ringer's solution. For region of interest (ROI) analysis, the area of single synapse and a part of single cell body were chosen (OS, outer segment; IS, inner segment; CB, cell body; Syn, synapse). (B–D) High KCl solution was applied to the retinal slice during a time-series recording. Due to the bath perfusion configuration, KCl responses were delayed by ~45 s. Six images at GCaMP6s channel (B), mCherry (C), and pseudocolor ratiometric images (D) were chosen to display calcium influxes in multiple synapses (small white arrows) and cell bodies of rod photoreceptors over time. (E–G) ROI analysis of GCaMP6s (E), mCherry (F), ratio (G) against time. The black arrowheads indicate images in B, C, and D. (H) Inner and outer segment of rod photoreceptors expressed GCaMP-R-6s. Average images of GCaMP6s and mCherry obtained in Ringer's solution. ROIs for inner segments were designated numbers 3, 4, and 5, and ROIs for outer segments were designated numbers 1, 2, and 6. (I–K) ROI analysis at the inner and outer segment (I, GCaMP6s; J, mCherry; K, ratio). Scale bars, 25 μm.

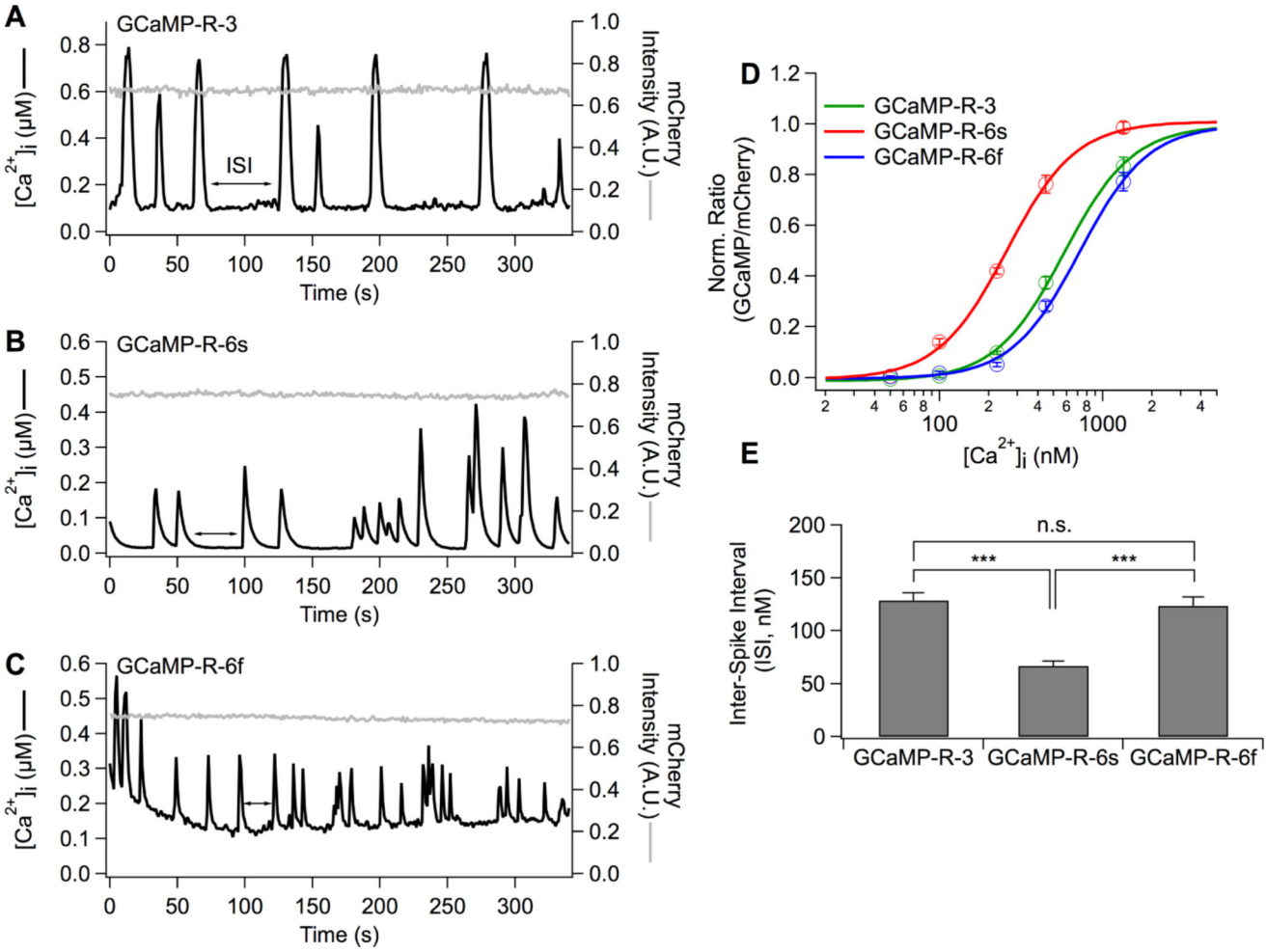

Figure 6.

Conversion of ratios into intracellular free calcium concentrations. (A–C) GCaMP-R variants were expressed in AtT20 cells (A, GCaMP-R-3; B, GCaMP-R-6s; C, GCaMP-R-6f). The three AtT20 cells showed spontaneous calcium fluctuations in Ringer's solution. The ratios of GCaMP to mCherry intensity obtained at direct excitation of GCaMP and mCherry were converted into cytoplasmic free calcium concentrations using the following eq (eq 1), $[Ca^{2+}]i = \{(\beta K_D)^n \times (R - R_{min})/(R_{max} - R)\}^{1/n}$. β is defined as the ratio of Ca^{2+}-free to Ca^{+}-saturated intensity of the denominator fluorescence protein ($\beta = 1$). K_D and n are the apparent dissociation constant and Hill coefficient, respectively, and derived from D. (D) Normalized average ratios were calculated and plotted against free calcium concentrations. The data were fit to the Hill equation, $y = 1/\{1 + ([K_D]/[Ca^{2+}])^n\}$ (3-ER/K, $n = 61$; 6s-ER/K, $n = 55$; 6f-ER/K, $n = 38$). (E) Average calcium concentrations at interspike intervals (ISIs) in AtT20 cells expressing GCaMP variants (3-ER/K, $n = 7$; 6s-ER/K, $n = 10$; 6f-ER/K, $n = 12$). Mean ± SEM (***$p < 0.001$).